Applied Surface Science 305 (2014) 86–92

Contents lists available at ScienceDirect

Applied Surface Science

journal homepage: www.elsevier.com/locate/apsusc

Protective properties of magnetron-sputtered Ti coating on $CoSb_3$ thermoelectric material

Degang Zhao*, Min Zuo, Zhenqing Wang, Xinying Teng, Haoran Geng

School of Materials Science and Engineering, University of Jinan, Jinan 250022, China

ARTICLE INFO

Article history:
Received 3 October 2013
Received in revised form 27 February 2014
Accepted 27 February 2014
Available online 12 March 2014

Keywords:
Coating
Thermoelectric
CoSb3
Magnetron sputtering

ABSTRACT

In this study, protective Ti coatings were deposited on the $CoSb_3$ substrate by DC magnetron sputtering to prevent the sublimation of Sb. The microstructure of Ti coating was observed by SEM and AFM. The thermal aging behaviors of coated $CoSb_3$ samples were investigated through accelerated aging at 650 °C for 24 h. The results indicated that Ti coatings were columnar crystals and body-centered cubic structure. The preferred orientation of Ti film was along the crystal plane of (0 0 2). The thickness of Ti film increased with the deposition time increasing. The weight loss decreased with the thickness of Ti coating increasing. Compared with the uncoated $CoSb_3$ material, the degradation of thermoelectric properties for coated $CoSb_3$ samples decreased slowly after accelerated thermal aging test.

1. Introduction

Recently, thermoelectric (TE) material has attracted worldwide attention due to their potential applications in electronic cooling, waste heat recovery and special power generation [1–3]. The conversion efficiency of TE material is determined by the dimensionless figure of merit, $ZT = \alpha^2\sigma T/\kappa$, where α is the Seebeck coefficient, σ is the electrical conductivity, T is the absolute temperature, and κ is the total thermal conductivity. The total thermal conductivity is composed of an electron part (κ_E) and a phonon part (κ_L). Skutterudite compounds have been reported to have high ZT value and regarded as one of the most promising TE materials operating at elevated temperature [4,5]. Great progresses have been achieved in the improvement of TE properties, and larger ZT up to 1.7 at 850 K was obtained in $Ba_uLa_vYb_wCo_4Sb_{12}$ triple-filled skutterudites [6–8]. However, $CoSb_3$ material is vulnerable to decompose and Sb atoms could sublime from $CoSb_3$-based skutterudites at high temperature, which would change the composition of TE materials, finally leading to the degradation of the TE performance. Furthermore, the sublimation products can diffuse or condense on the cold-side of the TE unicouples, resulting in the electrical short circuit of TE device. The thermal decomposition or sublimation is the major reason for the degradation of skutterudite materials working at high temperature [9,10]. Therefore, it is essential to develop a protective coating to suppress the sublimation of Sb from $CoSb_3$-based skutterudites. So far, few studies about the coating for $CoSb_3$ material were reported. Cr-5Si thin layers onto $CoSb_3$ deposited by pulse magnetron sputtering was used to deter the degradation of skutterudite at elevated temperatures in air, but the thin layers lost the protection function at 600 °C [11]. Dong et al. fabricated the silica-based composite coatings on the surface of n-type $Yb_{0.3}Co_4Sb_{12}$ and p-type $CeFe_3CoSb_{12}$ skutterudites using hybrid silica sol as raw material [12,13]. However, the methods mentioned above are complex and the thickness of protective film is difficult to control. In brief, the aim of coating on skutterudites is to prevent the sublimation, or at least reduce it to an acceptably low level. As we know, besides a certain chemical inertness with Co or Sb element, the coefficient of thermal expansion (CTE) is also an important factor for a suitable protective coating which should have the CTE match with $CoSb_3$ material. The CTE of $CoSb_3$ and Ti is $(0.92–1.05) \times 10^{-5}\ K^{-1}$ and $(0.85–0.90) \times 10^{-5}\ K^{-1}$ when temperature ranges from 100 °C to 600 °C, respectively [14]. Therefore, Ti film is possibly an appropriate protective coating for $CoSb_3$ material.

In this study, a protective Ti coating was conveniently deposited on the $CoSb_3$ substrate by magnetron sputtering to prevent the sublimation of Sb. The microstructure and growth feature of Ti film were observed by SEM and AFM. As the $CoSb_3$-based generator generally works at about 500 °C, the accelerated thermal aging tests at 650 °C for 24 h were carried out. The effect of suppressing sublimation Sb of Ti film was evaluated by measuring the TE properties after accelerated thermal aging test. Related thermal aging behavior was attentively discussed. The results are expected to be beneficial to the development of $CoSb_3$-based TE generator.

* Corresponding author. Tel.: +86 531 82765790.
E-mail address: mse_zhaodg@ujn.edu.cn (D. Zhao).

http://dx.doi.org/10.1016/j.apsusc.2014.02.173
0169-4332/

Table 1
Deposition conditions of Ti layer on $CoSb_3$ substrate prepared by magnetron sputtering.

Ti coating	Ar pressure (Pa)	Current (A)	Voltage (V)	Time (min)	Temperature (°C)	Thickness (μm)
Coating 1	2.5×10^{-3}	0.5	310	15	200	2
Coating 2	2.5×10^{-3}	0.5	310	30	200	7
Coating 3	2.5×10^{-3}	0.5	310	45	200	10

2. Experimental procedure

The substrate material, $CoSb_3$ skutterudite material, was synthesized by melting, quenching, annealing process. Stoichiometric quantities of the constituent pure elements Co (99.97%, powder) and Sb (99.99%, powder) were weighed according to the mole ration, loaded in a quartz tube with carbon depositing on the inner wall, and sealed under a pressure of 0.1 Pa. The samples were melted at 1050 °C for 16 h and then was quenched in saltwater. The obtained solid product was ground into fine powder and then sintered into a dense solid by hot-pressing sintering (HPS) at 560 °C for 30 min in a graphite die. The specimens with 10 mm in diameter and 2 mm in thickness were produced by HPS. All the densities of $CoSb_3$ samples measured were higher than 98%. The $CoSb_3$ substrates were first ultrasonically cleaned in acetone for 10 min, and then dried by blowing hot air before being place in the deposition chamber.

Pulsed magnetron sputtering technique was used to deposit Ti thin films. A titanium target (purity better than 99.9%, Beijing Haipu Technology Co., Ltd.) of 74 mm diameter and 3 mm thickness was used to deposit protective films on $CoSb_3$ substrate by means of a specially designed DC magnetron sputtering system. During sputtering, the target-to-substrate distance was kept constant at 70 mm. The substrate temperature was kept constant at 200 °C. The flow rate of the argon (99.99% purity) was 50 standard cubic centimeter per minute (sccm). Pre-sputtering of the Ti target was performed for 3 min before each deposition. The deposition conditions and pulse parameters of magnetron sputtering in the present investigation are given in Table 1. By adjusting the sputtering time, the thickness of Ti film was controlled. The structural properties of Ti films were characterized by X-ray diffraction (XRD, Rigaku, Rint-2000). The surfaces morphology of Ti thin films on the $CoSb_3$ substrates was observed by field emission SEM (JEOL, JSM-6700F) and atomic force microscopy (AFM, SPA-300HV). The surface area and weight of the $CoSb_3$ samples were measured before each test. The weight loss divided by exposed surface area provided the weight loss per area. The $CoSb_3$ samples with Ti coating were sealed in quartz tubes and heated at a rate of 220 °C/h in the furnace to the aging temperature (650 °C). After keeping at the aging temperature for 24 h, the samples were cooled to room temperature in furnace naturally. The mass changes were calculated by the difference after and before the thermal duration tests from an electronic balance with an accuracy of 0.1 mg. In the measurement of weight loss, the $CoSb_3$ samples were 8 mm × 8 mm × 4 mm and all surfaces of $CoSb_3$ samples were deposited by Ti films. The measurements of Seebeck coefficient and electrical conductivity were carried out by the standard four-probe method (ULVAC-RIKO, ZEM-2) in a flowing Ar atmosphere. The rectangular $CoSb_3$ samples with Ti films (10 mm × 3 mm × 2 mm) were prepared by magnetron sputtering under the same conditions. Actually, the hot sides of thermoelectric elements usually need to be deposited by coating, just as shown in Fig. 1(a). The direction of thermal fluid and current flow is parallel with that of coating. Therefore, the electrical conductivity and Seebeck coefficient of $CoSb_3$ samples with Ti coating deposited on four side faces were measured, as shown in Fig. 1(b). Based on the same model displayed in Fig. 1(a), disk-type $CoSb_3$ specimens with the dimensions of 10 mm (diameter) and 1 mm (thickness) were prepared for thermal conductivity. There is no coating on the upper surface and lower surface of samples, as shown in Fig. 1(c). Thermal conductivity was measured by a laser flash method (NETZSCH, LFA427) in vacuum. All measurements were performed in a temperature range of 27–550 °C.

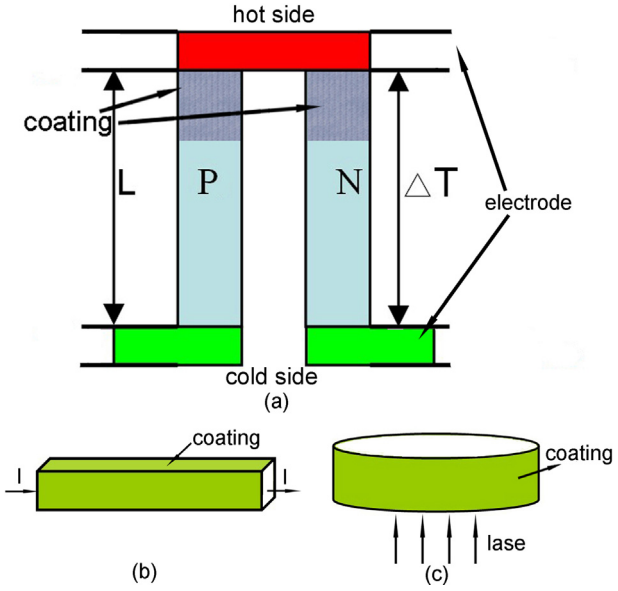

Fig. 1. (a) Schematic diagram of TE device; (b) schematic diagram of electrical conductivity of $CoSb_3$ with Ti coating; (c) schematic diagram of thermal conductivity of $CoSb_3$ with Ti coating.

3. Results and discussion

Fig. 2 shows the X-ray diffraction patterns of Ti coating on $CoSb_3$ substrate deposited by different time. Compared with the peaks of uncoated $CoSb_3$ samples, the peak of Ti (0 0 2) at $2\theta = 38.3°$ was observed in the XRD patterns of coated $CoSb_3$ samples. As the Ti film deposited by magnetron sputtering was very thin, the peaks of $CoSb_3$ substrate also existed. In addition, with the time of

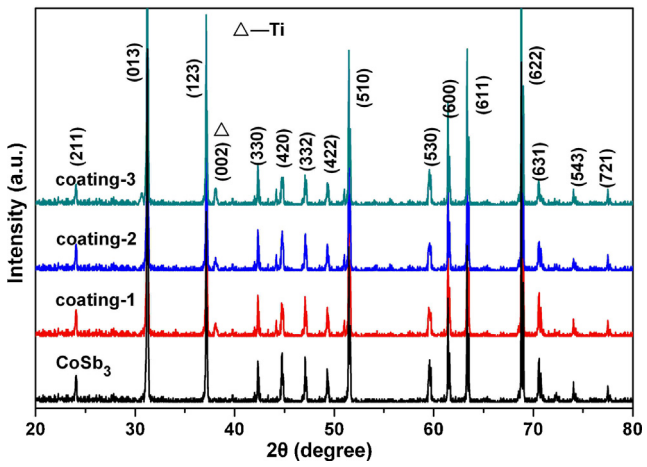

Fig. 2. XRD patterns of the as-deposited Ti films on $CoSb_3$ substrate.

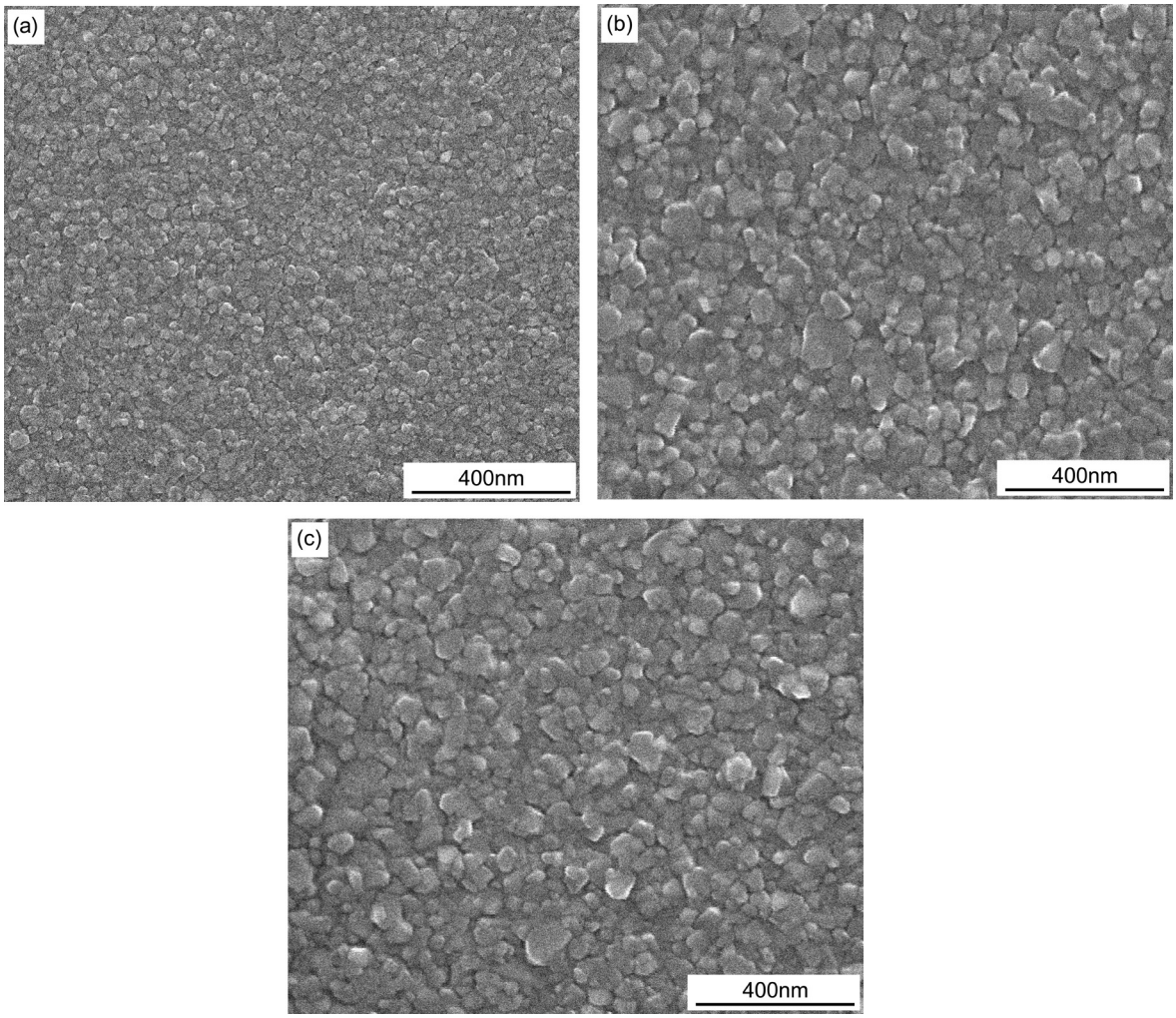

Fig. 3. Surface morphology of Ti film on $CoSb_3$ substrate after different deposition time using magnetron sputtering, (a) 15 min; (b) 30 min; (c) 45 min.

magnetron sputtering increasing, the intensity of peak of Ti increased which indicated the Ti thin film grew and the thickness increased. Fig. 3 shows the surface morphology of the Ti film on $CoSb_3$ substrate after different deposition time. It can be seen that no cracks, porosity or other defects existed on the Ti films. With the deposition time increasing, the grain size of Ti film increased. The average grain size of Ti film after 15 min was 30 nm, just as shown in Fig. 3(c). Moreover, the Ti thin film deposited grew in the mode of island growth. The formation of Ti thin film on the $CoSb_3$ substrate was the results of the deposition of sputtered atoms from the target on the $CoSb_3$ surface. Argon gas is ionized with the plasma and the argon ions are accelerated into the Ti target surface. Some of the Ti atoms are sputtered off of the target. As the temperature of substrate was relatively low, the sputtered Ti atoms were condensed on the $CoSb_3$ substrate. After the diffusion and migration of atoms, the stable crystal nucleuses formed and grew. Then the crystal nucleuses grew into islands. With the deposition time increasing, the islands became interconnected and the continuous Ti film formed on the substrate. The deposition rate was very slow in the initial stage due to the nucleation and growth of Ti thin film. With the deposition time increasing, the deposition rate increased and gradually became stabilized. Just as shown in Fig. 3, the Ti film became more smooth and denser with the deposition time increasing. The surface morphology of Ti film was also studied by AFM, as shown in Fig. 4. It also can be observed that the deposition of Ti film was the three-dimensional island growth. Several groups reported

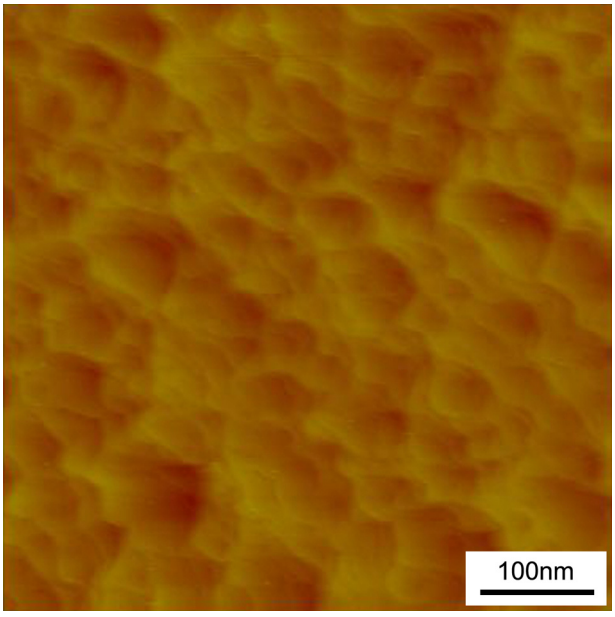

Fig. 4. AFM image of Ti film on $CoSb_3$ substrate after deposition of 45 min.

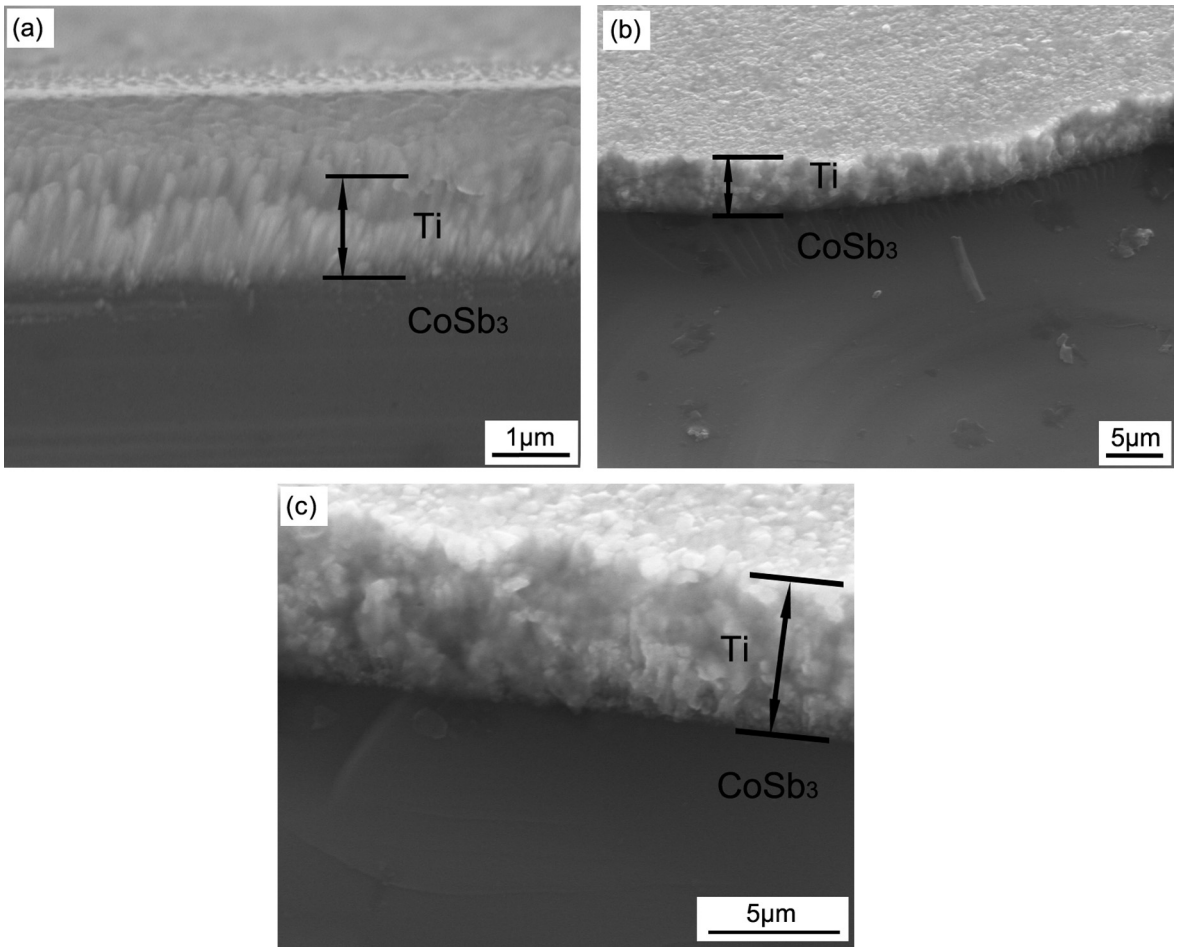

Fig. 5. (a) Fractural morphology of Ti film on $CoSb_3$ substrate after deposition of 15 min; (b) fractural morphology of Ti film after deposition of 30 min; (c) enlarged morphology of (b).

the lattice mismatch between film and substrate might affect the formation of surface islands [15,16], which was accounted for using the thermal dynamic and kinetic model [17,18]. Due to the low lattice mismatch between Ti and $CoSb_3$ [19], island growth of Ti film was distinct relatively. Fig. 5 shows the fractural morphology of the Ti film on $CoSb_3$ substrate deposited by different time using magnetron sputtering. It can be observed that the Ti film was a columnar grain structure and the thickness of Ti film was 1.2 μm after the deposition of 15 min. With the deposition time increasing, the thickness of Ti film increased to 5.8 μm after the deposition of 30 min. According to the zone model, the microstructure of sputter-deposited film was closely related to the T_s/T_m, where T_s is the substrate temperature and T_m is the melting point of film [20]. Based on the T_s/T_m, the structure zone could be divided into four regimes, in which the microstructure of sputtered film is critically affected by shadowing, surface diffusion and bulk diffusion with the T_s/T_m increasing. In this study the T_s/T_m for Ti film grown at 200 °C was about 0.24, which corresponds to the zone where surface and self-diffusion become active. As the surface diffusion of condensed atoms is high and the bulk diffusion is not sufficient, the film would grow in the form of columnar grains, which was also consistent with previous reports about the microstructure of sputter-deposited films [21,22].

As the hot sides of skutterudite-based TE materials generally work at about 500 °C, the accelerated thermal aging test of coated $CoSb_3$ samples was carried out at 650 °C for 24 h in this study. For comparison, the uncoated $CoSb_3$ sample was also tested through accelerated thermal aging test. Fig. 6 shows the SEM images of uncoated and coated $CoSb_3$ samples after accelerated thermal aging test. It can be seen that the surface of $CoSb_3$ became degraded seriously and some polyhedron crystallites (antimony) were precipitated in the grain boundary, just as shown in Fig. 6(a). The antimony in $CoSb_3$ sample sublimed according to the following equation [14]:

$$CoSb_3 = CoSb_2 + Sb(g)$$

However, no crack was found at the region of Ti/$CoSb_3$ interface in the coated $CoSb_3$ sample after accelerated thermal aging test, which indicated that the bonding of Ti coating with $CoSb_3$ substrate was well after accelerated thermal aging test, just as shown in Fig. 6(b). In addition, it is worth mentioning that some intermetallic phases such as Ti–Sb, Co–Ti or Ti–Co–Sb compounds maybe form at the region of Ti/$CoSb_3$ interface due to the interdiffusion during the thermal aging. If the cracks appear at the region of intermetallic phases due to the thermal stress after thermal aging test, the cracks will provide short-circuit channels of sublimation of Sb. In view of evaluating the protective effect of Ti coating, the intermetallic phases also play an important role in evaluating the lifetime of Ti coating on $CoSb_3$ materials. These experimental and theoretical studies are undergoing now and will be reported in future.

To evaluate the effects of Ti coating on suppressing the sublimation of Sb, the weight loss and TE properties of coated $CoSb_3$ samples after accelerated thermal aging test were measured. Fig. 7 shows the weight loss per unit area of coated $CoSb_3$ samples after accelerated thermal aging test. It can be seen that the weight loss

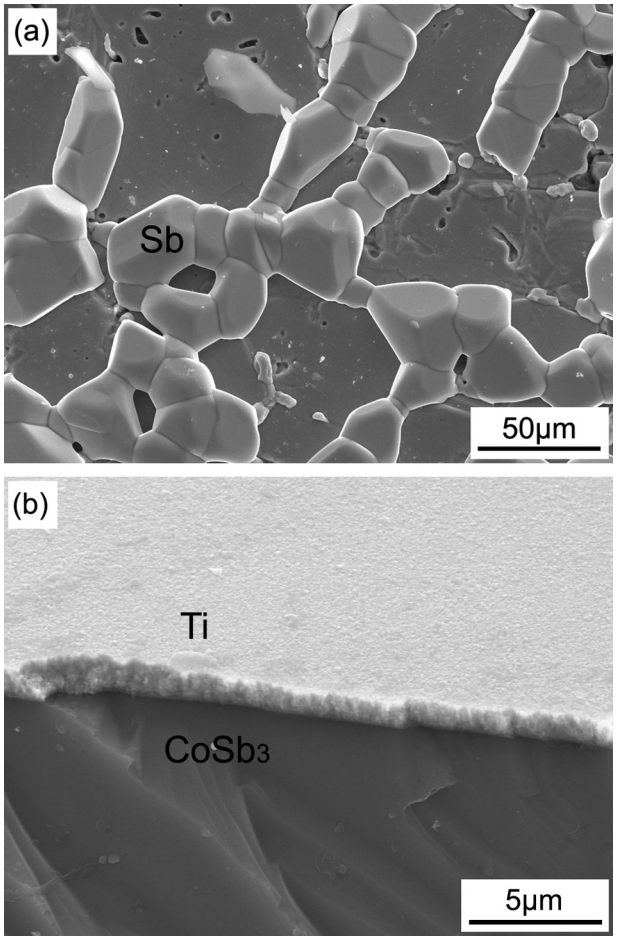

Fig. 6. (a) SEM image of uncoated $CoSb_3$ sample after accelerated thermal aging test; (b) SEM image of Ti film on $CoSb_3$ substrate after accelerated thermal aging test.

per unit area of coated $CoSb_3$ samples was much lower than that of uncoated $CoSb_3$ samples after accelerated thermal aging test, indicating the Ti coating could effectively suppress the sublimation of Sb in $CoSb_3$ materials. The weight loss per unit area of coated $CoSb_3$ samples with coating-1 was 2.3×10^{-2} kg/m^2 after accelerated thermal aging test. Moreover, protective effect of thicker Ti coating was better. The weight loss per unit area of coated $CoSb_3$ samples with coating-3 was 40% lower than that of coated $CoSb_3$ samples with coating-1 after accelerated thermal aging test.

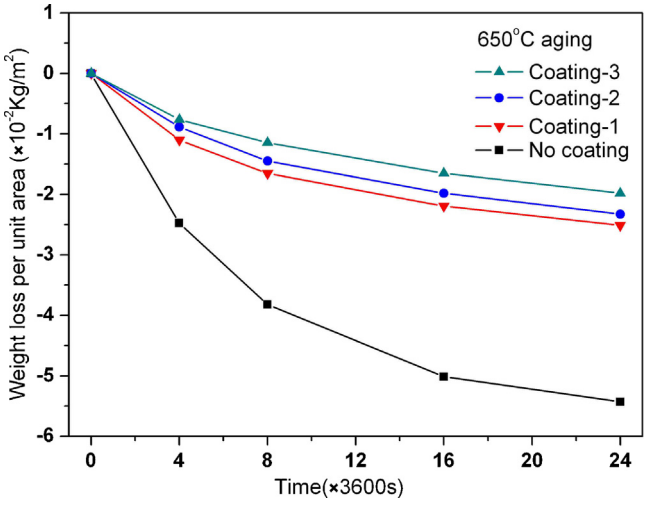

Fig. 7. The weight loss per unit area of coated $CoSb_3$ after accelerated thermal aging test.

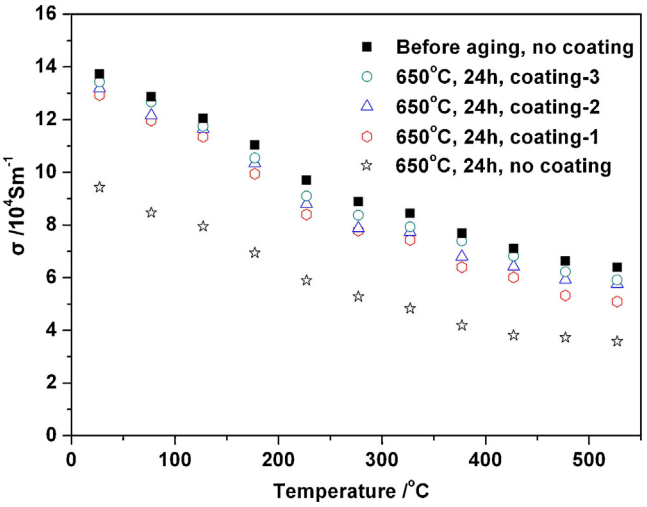

Fig. 8. The electrical conductivity of coated $CoSb_3$ after accelerated thermal aging test.

Fig. 8 shows the electrical conductivity (σ) of coated $CoSb_3$ samples after accelerated thermal aging test. Compared with the σ of uncoated $CoSb_3$ before accelerated thermal aging test, the σ of uncoated $CoSb_3$ after accelerated thermal aging test decreased by about 40%. However, the σ of coated $CoSb_3$ samples decreased a little bit compared with the σ of uncoated $CoSb_3$ before accelerated thermal aging test, except for an obvious decrease at high temperature region. The results indicated the Ti coating on $CoSb_3$ substrate could significantly hinder the sublimation of Sb and no other negative effects on the σ of $CoSb_3$. In addition, the thicker Ti coating on $CoSb_3$ substrate had the better protective effect on hindering the sublimation of Sb. Similar variation were also found in the results of Seebeck coefficient (α) of $CoSb_3$ with Ti coating after accelerated thermal aging test, just as shown in Fig. 9. Compared with the α of uncoated $CoSb_3$ before accelerated thermal aging test, the α of uncoated $CoSb_3$ after accelerated thermal aging test decreased by about 30%. Similarly, the α of coated $CoSb_3$ decreased a little bit compared with the α of uncoated $CoSb_3$ before accelerated thermal aging test. Fig. 10 is the thermal conductivity (κ) of coated $CoSb_3$ samples after accelerated thermal aging test. It can be seen that after accelerated thermal aging test, the κ of uncoated $CoSb_3$

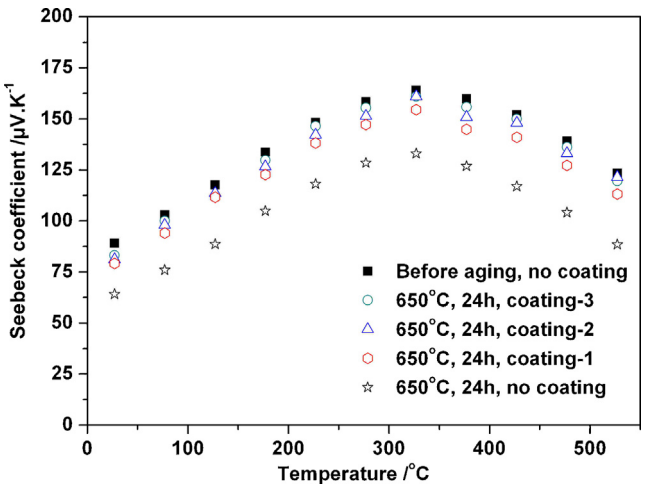

Fig. 9. Seebeck coefficients of coated $CoSb_3$ after accelerated thermal aging test.

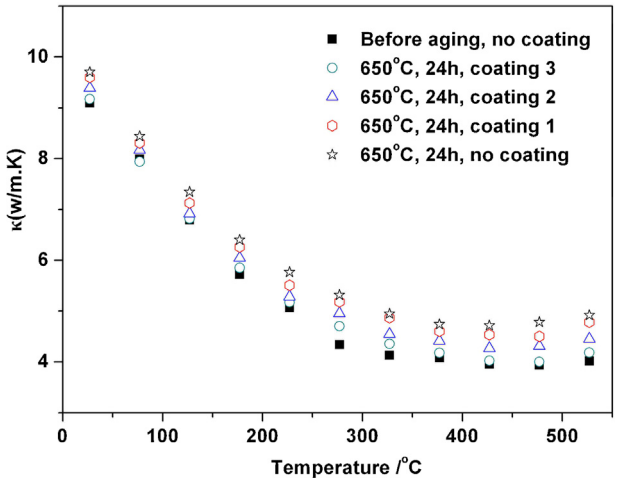

Fig. 10. The thermal conductivity of coated $CoSb_3$ after accelerated thermal aging test.

increased due to the higher κ of $CoSb_2$ resulting from the sublimation of Sb. However, the κ of coated $CoSb_3$ samples increased slowly compared with the κ of uncoated $CoSb_3$ samples because the sublimation of Sb was inhibited effectively. As the κ was measured according to the schematic diagram in Fig. 1 and there was no coating on the upper and lower surfaces, the direction of thermal fluid was parallel with that of coating. Therefore, the Ti coating may also contribute to the increased κ compared with the κ of uncoated $CoSb_3$ samples.

The conversion efficiency of TE materials depends on the maximum dimensionless figure of merit (*ZT*). From the measured electrical and thermal transport properties, the dimensionless figure of merit of coated $CoSb_3$ samples is calculated and shown in Fig. 11. Compared with the *ZT* value of uncoated $CoSb_3$ before accelerated thermal aging test, the *ZT* value of uncoated $CoSb_3$ decreased obviously after accelerated thermal aging test. However, the *ZT* value of coated $CoSb_3$ samples decreased unclearly after accelerated thermal aging test because the sublimation of Sb was suppressed due to the Ti coating. For the coated $CoSb_3$ samples with coating-3, the maximum *ZT* value decreased from 0.26 to 0.22 at 327 °C after accelerated thermal aging test.

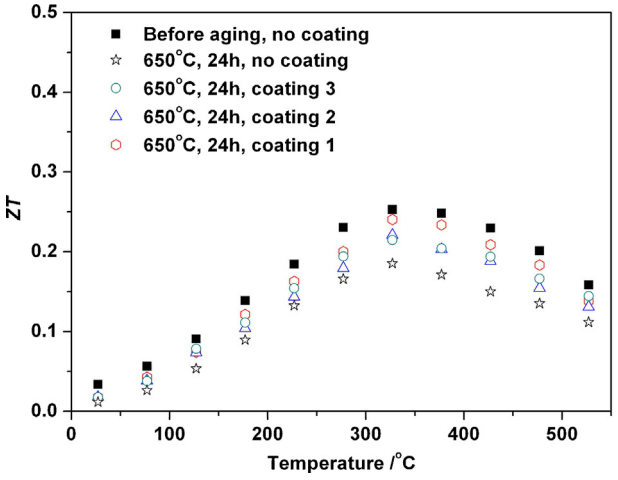

Fig. 11. The dimensionless figure of merit of coated $CoSb_3$ after accelerated thermal aging test.

4. Conclusions

Protective Ti coating was deposited on the $CoSb_3$ substrate by DC magnetron sputtering to prevent the sublimation of Sb. The preferred orientation of Ti film was along the crystal plane of (0 0 2). No cracks, porosity or other defects exist on the Ti films and the Ti film grew in the mode of island growth. The thickness of Ti film increased with the deposition time increasing. The coated $CoSb_3$ sample with thicker Ti film had lower weight loss per unit area after accelerated thermal aging test. Compared with the uncoated $CoSb_3$ material, the degradation of TE properties of coated $CoSb_3$ decreased slowly after accelerated thermal aging test.

Acknowledgments

The authors would like to thank the help from Shanghai Institute of Ceramics, Chinese Academy of Sciences and Shandong University for the measurement of TE properties. Financial supports from the National Natural Science Foundation of China (51202088 and 51271087), Shandong Provincial Natural Science Foundation of China (ZR2013EML004), Shandong Province Higher Educational Science and Technology Program (J13LA53), Shandong Provincial Doctoral Fund (BS2013CL004) and Doctoral Fund of University of Jinan (XBS1232) are acknowledged.

References

[1] F.J. Disalvo, Thermoelectric cooling and power generation, Science 285 (1999) 703–705.
[2] B.C. Sales, D. Mandrus, R.K. Williams, Filled skutterudite antimonides: a new class of thermoelectric materials, Science 272 (1996) 1325–1329.
[3] Z.K. Cai, P. Fan, Z.H. Zheng, P.J. Liu, T.B. Chen, X.M. Cai, J.T. Luo, G.X. Liang, D.P. Zhang, Thermoelectric properties and micro-structure characteristics of annealed N-type bismuth telluride thin film, Appl. Surf. Sci. 280 (2013) 225–228.
[4] H. Scherrer, L. Vikhor, B. Lenoir, A. Dauscher, P. Poinas, Solar thermoelectric generator based on skutterudites, J. Power Sources 115 (2003) 141–147.
[5] G. Rogl, Z. Aabdin, Effect of HPT processing on the structure, thermoelectric and mechanical properties of $Sr_{0.07}Ba_{0.07}Yb_{0.07}Co_4Sb_{12}$, J. Alloys Compd. 537 (2012) 183–189.
[6] X. Shi, J. Yang, J.R. Salvador, R. James, Multiple-filled skutterudites: high thermoelectric figure of merit through separately optimizing electrical and thermal transports, J. Am. Chem. Soc. 133 (2011) 7837–7840.
[7] Y.T. Qiu, L.L. Xi, X. Shi, L. Chen, Charge-compensated compound defects in Ga-containing thermoelectric skutterudites, Adv. Funct. Mater. 23 (2013) 3194–3198.
[8] L.L. Xi, J. Yang, C.F. Lu, L. Chen, W.Q. Zhang, Systematic study of the multiple-element filling in caged skutterudite $CoSb_3$, Chem. Mater. 22 (2010) 2384–2388.
[9] D. Zhao, C. Tian, S. Tang, Y. Liu, L. Chen, High temperature oxidation behavior of cobalt triantimondide thermoelectric material, J. Alloys Compd. 504 (2010) 552–556.
[10] H.H. Saber, M.S. El-Genk, T. Caillat, Effects of metallic coatings on the performance of skutterudite-based segmented unicouples, Energy Convers. Manage. 48 (2007) 555–560.
[11] E. Godlewska, K. Zawadzka, K. Mars, K. Mania, A. Wojciechowski, Opoka, Protective properties of magnetron-sputtered Cr–Si Layers on $CoSb_3$, Oxid. Met. 74 (2010) 205–210.
[12] H. Dong, X. Li, Y. Tang, J. Zou, L. Chen, Fabrication and thermal aging behavior of skutterudites with silica-based composite protective coatings, J. Alloys Compd. 527 (2012) 247–251.
[13] H. Dong, X. Li, X. Huang, Y. Zhou, W. Jiang, L. Chen, Improved oxidation resistance of thermoelectric skutterudites coated with composite glass, Ceram. Int. 39 (2013) 4551–4557.
[14] D. Zhao, C. Tian, S. Tang, Y. Liu, L. Chen, High temperature sublimation behavior of antimony in $CoSb_3$ thermoelectric material during thermal duration test, J. Alloys Compd. 509 (2010) 3166–3170.
[15] K.A. Aissa, A. Achour, J. Camus, Comparison of the structural properties and residual stress of AlN films deposited by dc magnetron sputtering and high power impulse magnetron sputtering at different working pressures, Thin. Solid. Films 550 (2014) 264–267.
[16] D.E. Jesson, G. Chen, K.M. Chen, S.J. Pennycook, Self-limiting growth of strained faceted islands, Phys. Rev. Lett. 80 (1998) 5156–5159.
[17] J. Tersoff, R.M. Tromp, Shape transition in growth of strained islands: spontaneous formation of quantum wires, Phys. Rev. Lett. 70 (1993) 2782–2785.

[18] D.E. Jesson, K.M. Chen, S.J. Pennycook, Kinetic pathways to strain relaxation in the Si–Ge system, MRS Bull. 21 (1996) 31–37.
[19] D.G. Zhao, X.Y. Li, W. Jiang, L. Chen, Interfacial evolution behavior and reliability evaluation of $CoSb_3$–Ti–MoCu thermoelectric joints during accelerated thermal aging, J. Alloys Compd. 477 (2009) 425–429.
[20] J.A. Thornton, High rate thick film growth, Annu. Rev. Mater. Res 7 (1977) 239–260.
[21] D.J. Kim, B.S. Kim, H.K. Kim, Effect of thickness and substrate temperature on the properties of transparent Ti-doped In_2O_3 films grown by direct current magnetron sputtering, Thin. Solid. Films 547 (2013) 225–229.
[22] Y.Y. Zhang, F. Feng, K. Shi, H.P. Lu, S.Z. Xiao, W. Wu, R.X. Huang, T.M. Qu, X.H. Wang, Z. Wang, Z.H. Han, Surface morphology evolution of CeO_2/YSZ (0 0 1) buffer layers fabricated via magnetron sputtering, Appl. Surf. Sci. 284 (2013) 150–154.